**Chemical interactions between silver nanoparticles and thiols - a comparison of mercaptohexanol against cysteine**

**TOH Her Shuang, BATCHELOR-MCAULEY Christopher, TSCHULIK Kristina, COMPTON Richard G.**

Department of Chemistry

Physical and Theoretical Chemistry Laboratory

University of Oxford, South Parks Road, Oxford OX1 3QZ, UK

E-mail: Richard.Compton@chem.ox.ac.uk

**Abstract**

The interaction between citrate capped silver nanoparticles and two different thiols, mercaptohexanol (MH) and cysteine, was investigated. The thiols interacted with silver nanoparticles in a significantly constrasting manner. With MH, a sparingly soluble silver(I) thiolate complex $AgSR_m$ ($R_m$ = $-(CH_2)_6OH$) was formed on the silver nanoparticle surface. Cyclic voltammograms and UV-vis spectra were used to infer that the $AgSR_m$ complex on the nanoparticle surface undergoes a phase transition to give a mixture of $AgSR_m$ and $Ag_2S$-like complexes. In contrast, when silver nanoparticles were exposed to cysteine, the citrate capping agent on the silver nanoparticles was replaced by cysteine to give cysteine capped nanoparticles. As cysteine capped nanoparticles form, the electrochemical data displayed a decrease in oxidative peak charge but the UV-vis spectra showed a constant signal. Therefore, cysteine capped nanoparticles were suggested to have either inactivated the silver surface or else promoted detachment from the electrode surface.

## 1 Introduction

Silver exists as silver metal and silver ions of different oxidation states of +1, +2, +3 and +4.[1] The most common states of silver are silver(0) metal and silver(I) ion and both of them interact with thiols in their own complex manner. A well known reaction of silver metal is the tarnishing of silverware to form silver(I) sulphide. It was discovered in 1930 that apart from the presence of hydrogen sulphide gas, oxygen is also required in this reaction: [2,3]

$$4\ Ag + 2\ H_2S + O_2 \rightarrow 2\ Ag_2S + 2\ H_2O \qquad (1)$$

The role of oxygen varies from the intermediate formation of silver(I) oxide to being the hydrogen acceptor to form water or hydroxide ions.[2,3] The overall reaction of silver tarnishing is concluded to form the product silver sulphide ($Ag_2S$) but there are case specific mechanisms depending on conditions such as pH, oxygen level, ultraviolet light presence and moisture levels.[2-4]

Silver(I) ion complexes with both inorganic and organic thiols with no redox reaction involved. With inorganic thiols like $HS^-$ and $S^{2-}$, it is possible to form many species such as AgSH, $[Ag(SH)_2]^-$ and $[Ag_2(SH)_2S]^{2-}$ depending on the concentration of the anions present.[5] With organic thiols, silver(I) ion forms the thermodynamically favourable complex of silver(I) thiolate (AgSR) with log $K_f$ ~ 13 $mol^2\ dm^{-6}$.[5] Silver(I) thiolate compounds, depending on the substituent group, are able to form polymer chains with various structures and formulas. A linear chain polymer is favoured with linear substituent group while a double helix-like structure is favoured with bulky side groups. [5,6] For cysteine and glutathione, they form polymers with various silver to thiol ratios.[7]

It is known that silver nanoparticle properties differ from those of the bulk metal and thus the interaction between silver nanoparticles and thiols may vary from bulk silver and

silver(I) ions.[4,8-10] Silver nanoparticles have been widely utilised to exploit their novel properties (e.g anti-bacterial properties, catalysis and biosensing) and their possible risks (e.g toxicity and possible cancer risk) have been researched extensively.[11-27] With thiols, silver nanoparticles have been proposed to form various types of compounds with different structures.[28-30] One of the plausible reaction routes suggested for organothiols is: [28,29]

$$4\ RSH + 4\ Ag + O_2 \rightarrow 4\ AgSR + 2\ H_2O \qquad (2)$$

It has been shown that with organothiols, AgSR remained on the surface, forming a shell, as evidenced by scanning electron microscopy.[28] Battocchio *et al.* suggested a shell of more than one species of silver thiolates – a mix of AgSR and $Ag_2S$-like complexes were formed when aromatic organothiols were added during silver nanoparticle synthesis.[30] In the typical environmental setting with plenty of oxygen, moisture and naturally existing thiols, given sufficient time, the final product of redox reaction of silver nanoparticles and thiols in the environment is speculated to be $Ag_2S$ with many possible intermediates such as AgSR.[3,5,28,29] Utilising the silver sulphide concept, water treatment plants have been proposed to make use of the naturally occurring thiols to transform silver nanoparticles into a harmless version of silver sulphide ($Ag_2S$) to combat the possible toxicity concerns brought by silver nanoparticles.[31,32] An important question that has to be answered is: Do the naturally existing thiols have the capability to convert silver nanoparticles into a final product of silver sulphide?

Beyond studying the basic interaction between silver nanoparticles and thiols, many analytical sensors exploited the strong silver-thiol affinity. UV-vis spectroscopy, fluorescence studies and electrochemical studies have all been employed as methods to monitor levels of cysteine, glutathione and silver nanoparticles.[10,21-24,33] Apart from for detection purposes,

cysteine and glutathione have also been employed as a capping agent for silver nanoparticles to prevent aggregation.[34,35] At alkaline pH, the negatively charged carboxylic group keeps the cysteine capped silver nanoparticles apart and hence stabilises them. However, in mildly acidic pH, when both the carboxylic acid and amino group are charged, they interact electrostatically, causing the silver nanoparticles to aggregate.[34]

As highlighted above, the reaction between silver nanoparticles and thiols is complicated. In the formation of polymeric silver(I) thiolates from silver(I) ions and thiols, the effect of the substituent groups is evident.[5-7] It may be anticipated that silver nanoparticles show different behaviour or interaction with different thiols. With the possibility of many products like $Ag_2S$ and AgSR and the complex kinetics and solubility constants that are involved, the question arises as to whether there is a general mechanism for silver-thiol interactions which can be applied to silver nanoparticles or if each thiol needs to be considered individually? Given that the interaction of silver nanoparticle and thiols is a redox reaction, electrochemical methods are naturally employed in the present work to determine if a general mechanism of silver-thiol interaction exists. UV-vis spectroscopy was also used in this study of silver nanoparticles to further support the electrochemical observations. Two different thiols are chosen to determine if they react in a similar way with silver nanoparticles. Mercaptohexanol (MH) is chosen as a model compound; its basic structure consists simply of a sulfhydryl group (-SH) and a hydroxyl group (-OH). The simple structure of this compound allows the study of the effect of thiol groups on silver and circumvents possible effect of other functional groups. In addition, cysteine is chosen as an analyte with strong biological importance. It acts as an antioxidant and a precursor to peptides like glutathione.[36,37] The considerable difference between MH and cysteine in

terms of silver-thiol interactions is explained in this article through electrochemical experiments and UV-vis studies. The voltammograms ascertain the changes in the ease and extent of oxidation of silver nanoparticles to silver(I) ions whilst the UV-vis spectra examine the changes in the nanoparticles' surface properties. Through this, a comparative view of silver-thiol interaction for MH and cysteine is presented.

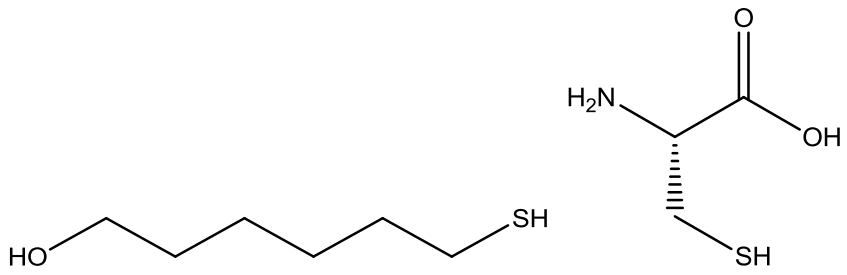


Figure 1. The chemical structures of mercaptohexanol and L-cysteine.

## 2 Experimental

### 2.1 Chemicals

Sodium nitrate (>99.5%, $NaNO_3$) was purchased from Fisons Scientific Equipment, Loughborough, UK. Trisodium citrate (>99%, $Na_3C_6H_5O_7$) and citric acid (99.7 %, $H_3C_6H_5O_7$) were supplied by BDH Laboratory Supplies, Poole, UK. Silver nitrate (>99%, $AgNO_3$), L-cysteine (97%, $C_3H_7NO_2S$) and sodium borohydride (99%, $NaBH_4$) were ordered from Sigma-Aldrich, Dorset, UK. Concentrated nitric acid (>70%, $H_2SO_4$) and hydrochloric acid (~37%, HCl) were supplied by Fisher Scientific, Loughborough, UK. 6-mercapto-1-hexanol (≥ 97%, $HO(CH_2)_6SH$) was obtained from Fluka Chemicals, Gillingham, UK. Sodium sulphide nonahydrate ($Na_2S.9H_2O$) was supplied by Acros Organics, Geel, Belgium. All solutions were made with ultrapure water from Millipore with resistivity not less than 18.2 MΩ.cm at 298K. All solutions were also degassed with nitrogen for 15 minutes thoroughly for both electrochemical and UV-vis spectroscopy experiments.

## 2.2 Nanoparticle synthesis and characterisation

Silver nanoparticles capped with citrate were synthesised using the method developed by Wan et al.[38] Two different batches of silver nanoparticles were synthesized and the smaller nanoparticles have a total silver concentration of 1.0 mM in the suspension and are sized as having radii of 4.7 ± 1.8 nm by transmission electron microscope as reported in a previous paper.[39] The bigger nanoparticles were synthesized through seeded growth synthesis. They have a total silver concentration of 3.1 mM in the suspension and are sized by scanning electron microscope as 13.6 ± 3.7 nm in radii.[40] All glassware were cleaned thoroughly with aqua regia (a mixture of concentrated hydrochloric acid and concentrated nitric acid in 3:1 ratio) prior to silver nanoparticle synthesis. The detailed synthesis procedure is given in the Supporting Information.

## 2.3 Voltammetry

A three electrode system in a Faraday cage was used for all electrochemical experiments. A μAutolab II from Metrohm-Autolab BV, Utrecht, The Netherlands was chosen as the potentiostat. The working electrode was a glassy carbon electrode of 3.0 mm diameter from CH instruments, Austin, TX, USA. The electrode was polished to a mirror finish on diamond sprays from Kemet, Kent, UK in the sequence of size 3.0 μm, 1.0 μm and 0.1 μm. A standard MSE (mercury/mercurous sulphate reference electrode [$Hg/Hg_2SO_4$, $K_2SO_4$ (saturated)], +0.62 V vs standard hydrogen electrode) was obtained from BASi, Wesy Lafayette, IN, USA.[41] The counter electrode was a platinum mesh. All electrochemical measurements were thermostated at 25 ± 1 $^{o}$C.

### 2.4 Silver nanoparticle modified glassy carbon electrode

The silver nanoparticle suspensions of particles of radii 4.7 ± 1.8 nm and 13.6 ± 3.7 nm were diluted with ultrapure water by a factor of 10 and 31 respectively to ensure the diluted samples contain a total concentration of 0.1 mM of silver. 3 µL of the diluted nanoparticle suspension was drop cast onto the glassy carbon electrode and dried under a nitrogen flow. The electrode after drying was used immediately for electrochemical experiments. A cyclic voltammetry was swept starting from -0.3 V vs MSE to +0.5 V and then reductively to -1.8 V to perform the electrochemical experiments.

### 2.5 UV-vis spectroscopy

UV-vis spectroscopy was performed using a spectrometer (U-2001, Hitachi, Mannheim, Germany) with a wavelength scan from 700 nm to 250 nm at a scan rate of 400 nm $min^{-1}$. A tungsten iodide and a deuterium light source were used. For UV-vis analysis, the nanoparticle suspensions of radii 4.7 ± 1.8 nm and 13.6 ± 3.7 nm were diluted by a factor of 24 and 48 with ultrapure water respectively to obtain absorbance in the analytically meaningful range of below 1.

## 3 Results and discussion

Herein, the electrochemical and UV-vis spectroscopic results of the interaction between silver nanoparticles and thiols are summarised. The changes in silver nanoparticle oxidation and the silver nanoparticle surface plasmon peaks in presence of mercaptohexanol (MH) and cysteine are compared and contrasted.

### 3.1.1 Electrochemical oxidation of silver nanoparticles in the presence of mercaptohexanol

A silver nanoparticle modified glassy carbon electrode was electrochemically oxidised In the presence of the model compound MH. Cyclic voltammetry was performed by sweeping oxidatively from -0.3 V vs MSE with a degassed electrolyte containing MH and 0.1 M sodium nitrate at a scan rate of 0.05 V $s^{-1}$. Two batches of silver nanoparticles, measuring 4.7 ± 1.8 nm and 13.6 ± 3.7 nm respectively, were studied. In order to study the silver-thiol interaction, two different sets of experiments were performed. In the first set of experiments, the modified electrode was electrochemically oxidised *immediately* after the exposure to the electrolyte containing different concentrations of MH ranging from 1 – 100 μM. In the second set of experiments, the modified electrode was electrochemically oxidised *after* soaking in the MH containing electrolyte for a period ranging from 5 minutes to 16 hours.

In Figure 2, cyclic voltammograms of silver oxidation for the nanoparticles of radii of 13.6 ± 3.7 nm with increasing MH concentrations are presented. In the absence of MH, as depicted by the black dashed line in Figure 2, the silver nanoparticles bound to the working electrode were oxidatively stripped to give a signal at +0.05 V vs MSE. This oxidation resulted in the formation of aqueous silver(I) ions.[42] In the presence of MH, the oxidation potential shifted positively from 0 V vs MSE to +0.25 V vs MSE depending of MH concentration. The voltammograms of nanoparticles (radii = 4.7 ± 1.8 nm) with increasing MH concentration are shown in the Supporting Information Figure S1; similar electrochemical trends (increase in oxidation potential and appearance of split oxidation signals) were observed as for these

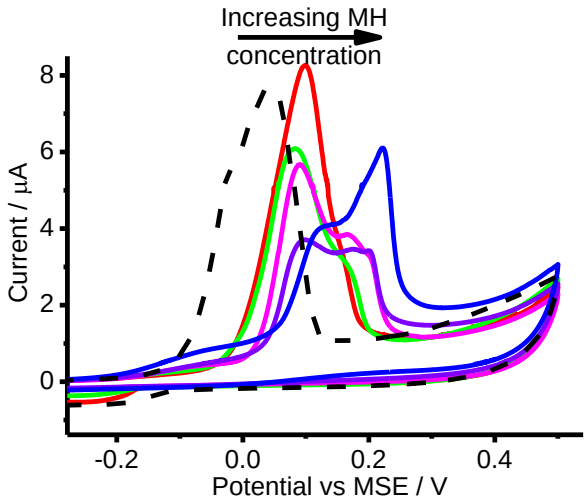


Figure 2. The oxidative stripping of silver nanoparticles with radii of 13.6 ± 3.7 nm from a glassy carbon electrode in 0.1 M sodium nitrate spiked with varying concentrations of mercaptohexanol measured at a scan rate of 0.05 V $s^{-1}$. Black dashed line: No mercaptohexanol; Red: 10 µM; Green: 25 µM; Pink: 50 µM; Purple: 75 µM; Blue: 100 µM.

smaller nanoparticles. The oxidative charge measured under the voltammetric signals can be related to the amount of metallic silver present on the electrode as described by Faraday's first law. The total oxidative charge under the voltammetric peaks for both batches of nanoparticles was measured and tabulated against the MH concentrations in Figure 3. As seen, the oxidative charges decreased when MH was added to the electrolyte. Thus, the amount of metallic silver available for electrochemical oxidation decreased in the presence of MH. Moreover, no significant difference was observed between the two nanoparticle batches as depicted in Figure 3. With increasing MH concentrations, the single oxidation signal split into two. As seen in Figure 2, the second oxidation signal at +0.25 V vs MSE grew in dominance as the concentration of MH increased.

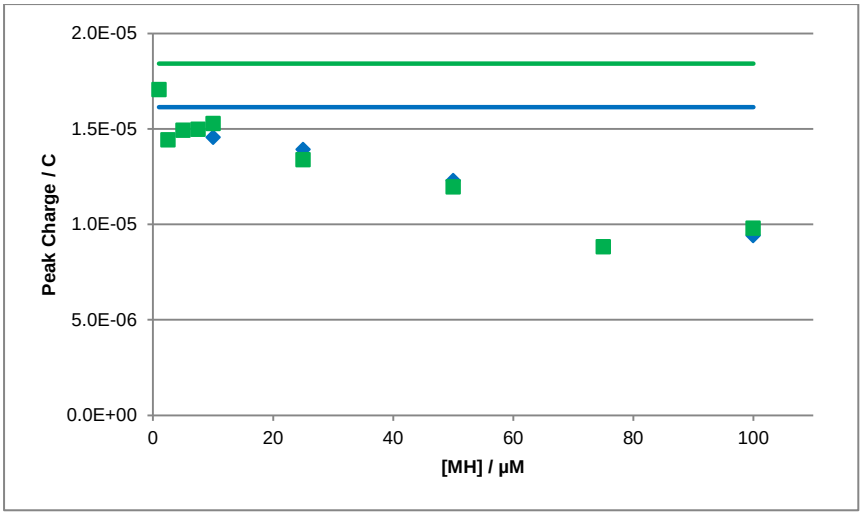


Figure 3. The oxidative stripping charge of silver nanoparticles from a glassy carbon electrode in 0.1 M sodium nitrate spiked with different concentrations of mercaptohexanol recorded at a scan rate of 0.05 V $s^{-1}$. The change in peak charge under the oxidation signals as different concentrations of mercaptohexanol were spiked in the electrolyte is shown. Nanoparticles of two different size distributions were used. Blue diamonds: silver nanoparticles of radii 4.7 ± 1.8 nm; Green squares: silver nanoparticles of radii 13.6 ± 3.7 nm. Solid lines: average peak charge under the oxidation signal when no mercaptohexanol is present.

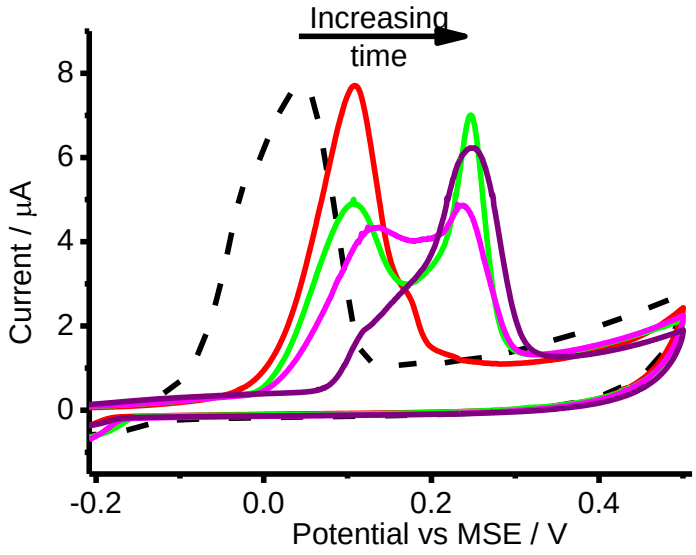


Figure 4a. The oxidative stripping of silver nanoparticles (radius = 13.6 ± 3.7 nm) from a glassy carbon electrode in 0.1 M sodium nitrate spiked with 10 µM mercaptohexanol with different exposure times recorded at a scan rate of 0.05 V $s^{-1}$. Black dashed: CV recorded immediately with NO mercaptohexanol; Red: CV recorded immediately with 10 µM mercaptohexanol; Green: CV recorded after electrode was exposed to 10 µM mercatohexanol for 15 minutes; Pink: 30 minutes; Purple: 16 hours.

In the time variation experiments, the silver nanoparticle (radii = 13.6 ± 3.7 nm) modified electrode was soaked in 0.1 M sodium nitrate containing 10 µM of MH for various times before electrochemical oxidation via cyclic voltammetry was performed. The voltammograms and oxidative peak charge underneath the signals are summarised

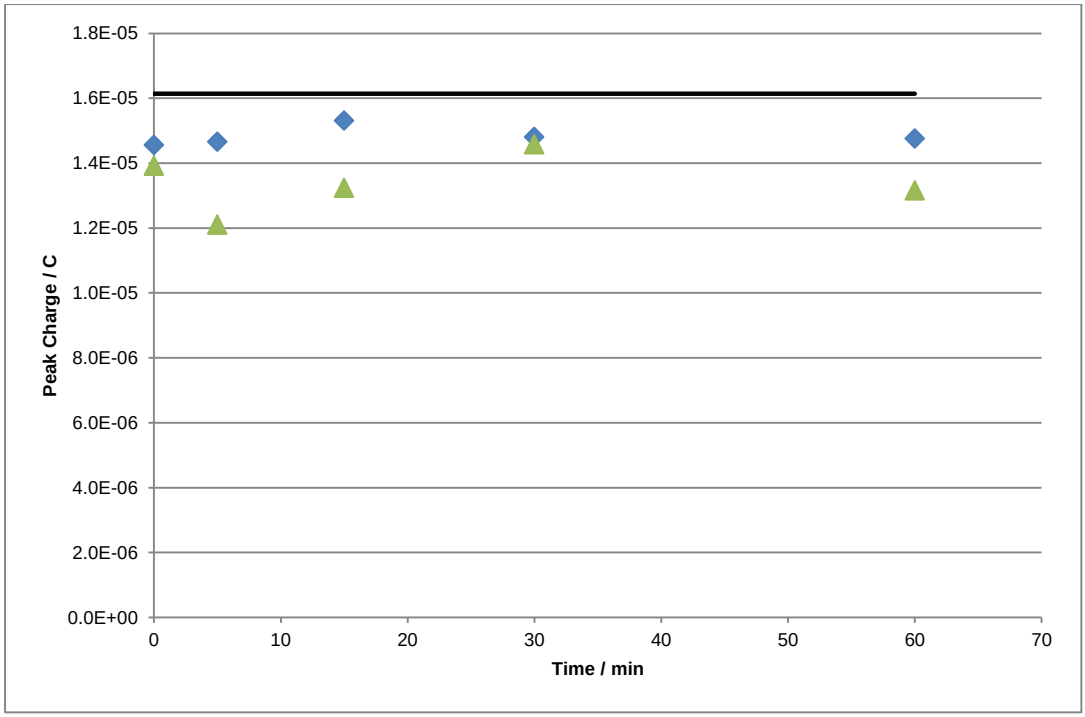


Figure 4b. The oxidative stripping of silver nanoparticles (radii = 13.6 ± 3.7 nm) from a glassy carbon electrode in 0.1 M sodium nitrate spiked with different amounts of mercaptohexanol measured at a scan rate of 0.05 V $s^{-1}$. The peak charge under the oxidation signal is plotted against the exposure time to mercaptohexanol. Blue diamonds: 10 µM mercaptohexanol in electrolyte; Green triangles: 25 µM mercaptohexanol in electrolyte. Solid line: peak charge under oxidation signal when no mercaptohexanol was added and the CV was recorded immediately.

respectively in Figure 4a and 4b. As seen in Figure 4a, increasing the MH exposure time gave rise to a split oxidation signal where the dominance of the second peak grew with time. Figure 4b shows the oxidative charges (obtained by integration under the peaks) remained relatively constant as the soaking time increased. Comparing the two sets of experiments involving varying concentrations and exposure times, there is a key difference between the two: the oxidative peak charge had a negative correlation with MH concentration (Figure 3) whilst the recorded peak charge remained effectively constant with exposure time (Figure 4b).

To explain the trends observed above, the existing literature research summarised within the introduction has to be considered. Knowing that AgSR and $Ag_2S$ are probable products in this redox reaction between silver nanoparticles and MH, therefore, two sets of control experiments involving AgSR and $Ag_2S$ were performed and detailed in the Supporting

Information Figure S2 and S3. The findings were as follow: First, mixing equal proportions of silver nitrate and MH gave a sparingly soluble white compound of $AgSR_m$ (where $R_m$ = -$(CH_2)_6OH$)). $AgSR_m$ did not give an oxidation signal in the electrochemical window of interest (0 V to + 0.3 V vs MSE). Second, to form $Ag_2S$, silver nanoparticles (radii = 13.6 ± 3.7 nm) were oxidised in the presence of $Na_2S$. The oxidative charge recorded under the signal decreased with increasing concentration of sodium sulphide. No split oxidation peaks was observed as silver sulphide, $Ag_2S$, was formed and the oxidation signal remained at the same potential.[43]

### 3.1.2 UV-vis spectroscopy data of silver nanoparticles in the presence of mercaptohexanol

To further support the electrochemical findings, UV-vis spectroscopy of silver nanoparticles in the presence and absence of MH was performed. Silver nanoparticles exhibit a surface plasmon peak around 400 nm in a UV-vis spectrum.[44] The surface plasmon peak is known to be sensitive to several factors such as size, capping agent, solvent and shape.[43-48] The difference in capping agent or coatings on silver nanoparticles can change the recorded surface plasmon signals.[43,46,48] Through the process of aggregation or increasing the size of silver nanoparticles, the surface plasmon peak red shifts.[44]

Similar to the electrochemical experiments, the two factors of concentration and time were varied. For the concentration experiments, both batches of silver nanoparticles were diluted and exposed to different concentrations of MH. In the time variation experiments, the nanoparticles of radii 4.7 ± 1.8 nm and 13.6 ± 3.7 nm were diluted by a factor of 24 and 48, spiked with 5 µM and 10 µM of MH and monitored over a period of 45 minutes and 15 minutes respectively. All the solutions were thoroughly degassed with nitrogen in both sets of experiments.

In the time study, as depicted in Figures 5a and 5b, without MH, a sharp surface plasmon peak at about 395 nm indicated the presence of silver nanoparticles.[44] As seen in Figure 5a, for the smaller silver NP (radii = 4.7 ± 1.8 nm), increasing MH exposure time caused the peak to broaden. Conversely, in Figure 5b, the bigger silver NP (radii = 13.6 ± 3.7 nm) had a drop in the absorbance peak at around 400nm and a new peak around 500-600nm appeared with increasing MH exposure time. For the concentration variation experiments, with increasing MH concentration, the effect of MH on the spectrum was the same as increasing MH exposure time. The spectra of increasing MH concentration are recorded in the Supporting

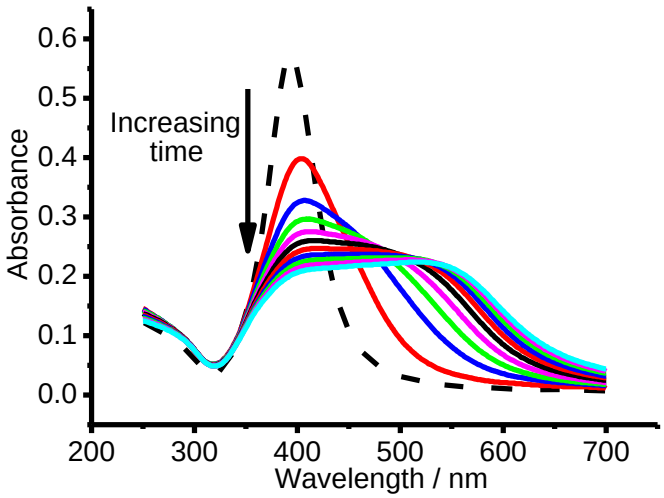


Figure 5a. UV-vis spectrum of silver nanoparticles (radii = 4.7 ± 1.8 nm) after exposure to 5 μM of mercaptohexanol for different amounts of time. Black dashed: No mercaptohexanol; Red: immediate. Blue: 5 mins. Cyan: 45 mins. Measurements were taken at intervals of 5 minutes for 45 minutes.

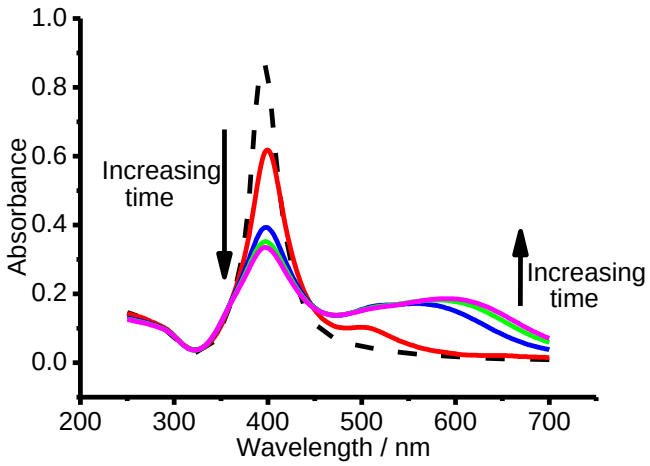


Figure 5b. UV-vis spectrum of silver nanoparticles (radii = 13.6 ± 3.7 nm) after exposure to 10 µM of mercaptohexanol for different amounts of time. Black dashed: No mercaptohexanol; Red: immediate; Blue: 5 mins; Green: 10 mins; Pink: 15 mins.

Information Figure S4 and S5. In addition, a control experiment was performed which demostrated that the growing second signal at around 500 – 600 nm was not caused by the formation of $Ag_2S$ (see in the Supporting Information Figure S6).[43] Hence, there are six major observations for the interaction between silver and MH to be accounted for, as follows.

I. The decreasing oxidative peak charge with increasing MH concentration (Figure 3)

II. The increase in electrochemical oxidation potential in the presence of MH (Figure 2)

III. The occurrence of the split electrochemical oxidation signal with increasing MH concentration or increasing exposure time (Figure 2 and 4a)

IV. The constant electrochemical oxidative charge with increasing MH exposure time (Figure 4b)

V. The *apparent* absence of a size effect in electrochemical experiments (Figure 3)

VI. The decreasing absorbance and change in UV-vis peak shape with increasing MH concentration or increasing exposure time (Figure 5a and 5b)

Taking all the observations into consideration, a overview of the silver-MH interaction is provided below, giving a full and consistent explanation.

### 3.1.3 The decreasing oxidative peak charge with increasing MH concentration

Thiols consume metallic silver by oxidising it to silver (I) to form silver-thiol complexes. This reaction concomitantly results in reduction products such as protons, hydrogen gas or water depending on pH and the availability of oxygen.[3,28] Hence, the cause of the decreasing peak charge is likely related to the redox reaction resulting in the formation of $AgSR_m$ or $Ag_2S$-like complexes (Figure 3).[30,49,50] Given that $AgSR_m$ is an intermediate in the formation of $Ag_2S$ -like complexes, it is likely that $AgSR_m$ formation is responsible for the initial drop in oxidative charges.[i] With different concentrations of MH, varying amounts of $AgSR_m$ are formed, leading to the difference in the measured peak charge.

### 3.1.4 The increase in the oxidation potential in the presence of MH

In the control experiments of AgSR and $Ag_2S$, no oxidation signal from +0.1 V to +0.3 V vs MSE was found (Section 3.1.1). Thus, the observed increase in oxidation potential is not due to silver being oxidised to form $AgSR_m$ or $Ag_2S$ (Figure 2 and 4a). Since neither $AgSR_m$ nor $Ag_2S$ is involved, the oxidation signal is related to the oxidation of silver to silver(I) ions. It is speculated that MH reacts with silver nanoparticles to give a shell of $AgSR_m$ as reported in the literature.[28] Given that $AgSR_m$ was observed to be a sparingly soluble solid in the control experiments (Section 3.1.1), $AgSR_m$ might form an insoluble shell which encapsulates the silver metal core. The trend of oxidation signal shifting to a higher oxidation potential (+ 0.1 V vs MSE) in the presence of MH can be explained by the slowed kinetics of silver nanoparticle oxidation due to the insoluble $AgSR_m$ shell.

[i] In this case, the $AgSR_m$ shell formed on the nanoparticle surface (reference 29) is suggested to be a solution phase chemical reaction and not detected electrochemically.

### 3.1.5 The occurrence of the split oxidation signal with increasing MH concentration or increasing exposure time

As described above, the oxidation of silver to silver(I) ions is the sole contributor to the observed oxidative peak charge since oxidation of silver to either $AgSR_m$ or $Ag_2S$ are not likely responsible for the oxidative charges (Section 3.1.4). Hence, the silver-MH interaction must have further obstructed the kinetics of silver oxidation to silver(I) ions to cause the observed split oxidation signals. From the previous Section 3.1.3, it was surmised that an insoluble $AgSR_m$ shell is formed on the nanoparticle surface. Battocchio *et al.* reported a mixture of AgSR and $Ag_2S$-like complexes was found in the shell that encapsulated the silver nanoparticles.[30] Therefore, it is possible that given time or sufficient MH concentration, the $AgSR_m$ shell may undergo a phase transition to form a compact shell with a mixture of $AgSR_m$ and $Ag_2S$-like complexes. Thus, the kinetics of silver oxidation would be further obstructed after this phase transition occurred. This would give rise to a split oxidation signal where the silver oxidation kinetics are hindered by two different extents – one by the insoluble shell of $AgSR_m$ (+0.1 V vs MSE) and another by the compact shell of AgSR and $Ag_2S$-like complexes (+0.25 V vs MSE). In addition, a phase transition can have a delayed onset compared to the quick formation of $AgSR_m$, hence the peak at +0.25 V gains dominance with increasing time and is more favoured when more MH is available.

### 3.1.6 The constant oxidative charge with increasing MH exposure time

With increasing exposure time to MH, the peak charge under the oxidation signals remained effectively constant as depicted in Figure 4b. Therefore, following Faraday's first law, no more metallic silver was oxidised by MH with increasing time. As suggested in Section 3.1.3, $AgSR_m$ is formed on the nanoparticle surface in the presence of MH. This sparingly soluble

shell of $AgSR_m$ can stop the approach of additional MH which diffuses to the surface with increasing exposure time. Thus, with increasing time, no additional $AgSR_m$ is formed, no more silver metal was consumed and the measured oxidative charge remained effectively constant with increasing MH exposure time.

### 3.1.7 The *apparent* absence of a size effect

As shown in Figure 3, two different batches of nanoparticles of radii 4.7 ± 1.8 nm and 13.6 ± 3.7 nm were used in the experiments. Given that the nanoparticles have different surface areas and $AgSR_m$ is speculated to form a shell on the nanoparticle surface, one might anticipate a possible difference in the decrease of the oxidative charges. However, no significant difference was found between the two batches of nanoparticles. It was observed in Figure 4b that the formation of $AgSR_m$ (drop in oxidative charge) occurred effectively instantaneously (time scale of at most a few seconds). It is surmised that the rate of $AgSR_m$ formation is controlled by the rate of MH diffusion to the surface. Considering the diffusional regime which occurs at this high silver surface coverage ($4.2 \times 10^{-5}$ mol $m^{-2}$), there is a complete overlap of the individual diffusional domains to give a linear diffusion profile across the entire working electrode.[51,52] In this linear diffusion regime, based on calculations, it takes less than one second to cover the surface with thiol through diffusion if the concentration of MH is at 10 μM.[53] Taking into account the convection caused by electrode insertion into the electrolyte, the actual time taken for MH to cover surface is even shorter. The short time which is required for thiol to diffuse to the surface and form $AgSR_m$ might explain the instantaneous drop in peak charge. Moreover, at this diffusion regime where there is a linear diffusion to the electrode, the amount of MH diffusing to the electrode surface is solely dependent on electrode area instead of nanoparticles' surface

area. Since the working electrode used for both batches of nanoparticles is the same, similar amounts of MH reached the electrode surface. This would result in similar amount of $AgSR_m$ formed, explaining the apparent indifference in the decrease of peak charge between both batches of nanoparticles in Figure 3. Hence, it is very probable that the interaction between silver nanoparticles and MH is a diffusional limited process.

### 3.1.8 The decreasing absorbance and change in UV-vis peak shape with increasing MH concentration or increasing exposure time

With increasing exposure time or MH concentrations, a broadening of the absorbance signal at 395nm was seen for nanoparticles of radii 4.7 ± 1.8 nm in Figure 5a. For the bigger nanoparticles (radii = 13.6 ± 3.7 nm), the absorbance signal at 395 nm decreases and a signal at 500 – 600 nm grows, as seen in Figure 5b. The red shift of an absorbance signal is often linked to an increase in size or aggregation.[10,44] The observations in the experiments may thus be related to aggregation. It is known that the larger the silver nanoparticles, the greater the red shift.[44] It was observed in Figure 5a and 5b that the red shift of the peak occurred to a different extent. If this was solely due to aggregation, one would expect the two different nanoparticle batches to have the same response as they both aggregate into large particles. Moreover, when the electrochemical data is considered, aggregation cannot explain the electrochemical trend of split oxidation signals seen in Figure 2 and 4a. It is known from previous literature that at this surface coverage where the linear diffusional regime across the electrode is dominant, the oxidation potential is solely dependent on the silver surface coverage instead of the size of nanoparticles.[51,54] If only aggregation was occurring, there should be a continuous size distribution with unchanged silver surface

coverage and thus no change in electrochemical oxidation potential should be observed. Hence, another process must have taken place to explain the observations.

The hypothesis of a phase transition supports the observations of split oxidation signals (Section 3.1.5) and the change in shape of the UV-vis signals. The work of A. Henglein established that a change in surface plasmon peak can be caused by different coatings on the silver nanoparticles surface.[43,46] The absorbance signal of silver nanoparticles with different thickness of silver oxide have been known to red shift to different extents.[48] This phenomenon supports the theory of a phase transition taking place, proposed in Section 3.1.5 where a phase transition causes the surface plasmon peak to occur at different wavelengths. Hypothesising that phase transition is a process where the $AgSR_m$ shell transforms into a shell containing $AgSR_m$ and $Ag_2S$-like complexes, there are two populations in the silver nanoparticles suspension during the UV-vis experiment. Hence, the signal at 400 nm could be attributed to the nanoparticles with $AgSR_m$ on the surface before phase transition. On the other hand, the absorbance peak at 500 – 600 nm may be linked to the nanoparticles that underwent phase transition. The phase transition could cause a change in shell composition, giving rise to two distinct populations to cause two separate signals where one of them is red shifted to 500 – 600 nm. The smaller silver nanoparticles (radii = 4.7 ± 1.8 nm) have a broadening signal instead of two distinct signals. It is known that the shell thickness may affect the degree of the red shift of surface plasmon signal.[48] As the two batches of silver nanoparticle differ in size, the $AgSR_m$ shell on the nanoparticle surface can be of different thickness, resulting in a milder extent of red shift of the surface plasmon peak. Therefore, from both UV-vis spectra and electrochemical observations, it is proposed that it is more likely that the phase transition of silver nanoparticles caused the change in

shape of absorbance peak instead of aggregation. In addition, given that the second signal did not appear in the control experiment of $Ag_2S$, it signifies that the substituent group on MH is crucial to phase transition even though it may not be directly involved in the silver-MH interaction.

### 3.1.9 Summary of the interaction between silver nanoparticles and mercaptohexanol

In summary, all six major observations are explained above with strong supporting evidence. First, the drop in oxidative charge with increasing MH concentration can be explained by the formation of $AgSR_m$ that consumes metallic silver. Second, the increase of oxidation potential in the presence of MH could be due to the formation of $AgSR_m$ on the nanoparticle surface which obstructs the oxidation process of silver to silver(I) ions. Third, the split oxidative peak with increasing MH concentration or exposure time can be explained by the instant formation of $AgSR_m$ on the nanoparticle surface which obstructs the silver oxidation kinetics, giving the first oxidation signal at +0.1 V vs MSE. A phase transition can occur with $AgSR_m$ on nanoparticle surface to form a compact layer of $AgSR_m$ and $Ag_2S$-like complexes which further hinder the kinetics of silver oxidation, giving rise to the second oxidation signal at +0.25 V vs MSE. Fourth, the constant oxidative charge with increasing MH exposure time may be explained by the instant formation of the sparingly soluble $AgSR_m$ shell which slows the approach of incoming MH and decreases the formation of $AgSR_m$ to a minimum. Thus, the oxidation of metallic silver is reduced to a minimum with increasing MH exposure time too. With increasing exposure time, it is suggested that only phase transition of $AgSR_m$

is occurring, resulting in a growing dominance of the second signal at +0.25 V vs MSE without decreasing the oxidative charge. Fifth, the linear diffusional regime of MH towards the electrode may cause similar amounts of MH to reach both batches of nanoparticles and hence, no apparent size effect is observed. Sixth, the spectroscopic data also supports the hypothesis of phase transition through the appearance of the second absorption signal at 500 – 600 nm.

### 3.2.1 Electrochemical oxidation of silver nanoparticles in the presence of cysteine

Cysteine here is chosen for the next part of the study. Analogous experiments between silver nanoparticles and cysteine were carried out to compare and contrast with silver-MH interaction. Thus, concentration and time studies were carried out with cysteine. For the concentration studies, an electrode modified with silver nanoparticles of either radii 4.7 ± 1.8 nm or 13.6 ± 3.7 nm was electrochemically oxidised in the presence of different concentrations from 10 nM to 1 mM of cysteine. Cyclic voltammetry was performed by sweeping oxidatively from -0.3 V vs MSE at a scan rate of 0.05 V $s^{-1}$ *once* the modified working electrode was exposed to the degassed 0.1 M sodium nitrate containing cysteine. The voltammograms of silver nanoparticles (radii = 4.7 ± 1.8 nm) exposed to increasing concentrations of cysteine are shown in Figure 6. The voltammogram for silver particles ( radii = 13.6 ± 3.7 nm) is found in Supporting Information S7. It is seen that the oxidation potential of silver to silver(I) ions remained essentially constant and split oxidation signals were not observed. In Figure 7, the oxidative peak charge measured (integration underneath the voltammetric signals) was plotted against the concentration of cysteine. Similar to MH, with increasing cysteine concentration, the peak charge decreased.

Considering the inherent variability of the experiments, it is not possible to show a significant difference between the two batches of nanoparticles. Hence, with increasing cysteine concentration, a decrease in oxidative peak charge, a constant oxidative potential and an absence of a split oxidation signal are reported. In contrast, the MH studies showed an increase in oxidation potential and the appearance of split oxidation signals with increasing MH concentration. Therefore, the two thiol compounds have mechanisms which differ from one another.

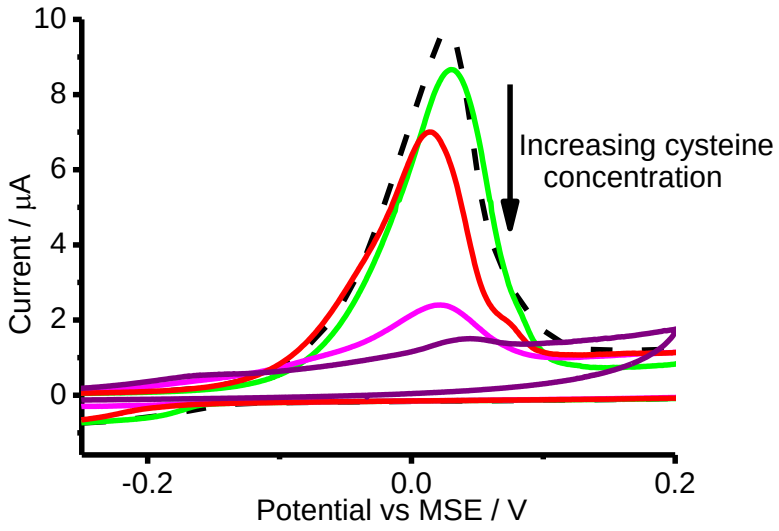


Figure 6. The oxidative stripping of silver nanoparticles (radii = 4.7 ± 1.8 nm) from a glassy carbon electrode in 0.1 M sodium nitrate spiked with different amounts of cysteine measured at a scan rate of 0.05 V $s^{-1}$. Black dashed line: 0 nM cysteine; Red: 500 nM; Green: 1 µM; Pink: 25 µM; Purple: 100 µM.

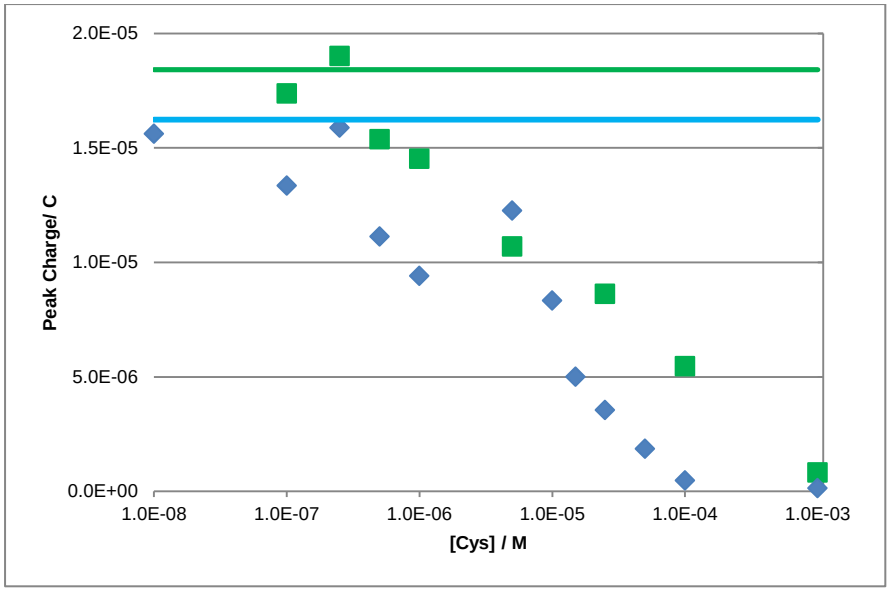


Figure 7. The oxidative stripping charge of silver nanoparticles from a glassy carbon electrode in 0.1 M sodium nitrate spiked with different amounts of cysteine measured at a scan rate of 0.05 V $s^{-1}$.The change in peak charge under the oxidation signal as different amounts of cysteine is spiked in the electrolyte. Nanoparticles of two different size distributions were used. Blue diamonds: silver nanoparticles of radii 4.7 ± 1.8 nm; Green squares: silver nanoparticles of radii 13.6 ± 3.7 nm. Blue line: average peak charge under the oxidation signal when no mercaptohexanol is present for nanoparticles of radii 4.7 ± 1.8 nm. Green line: average peak charge under the oxidation signal when no mercaptohexanol is present for nanoparticles of radii 13.6 ± 3.7 nm.

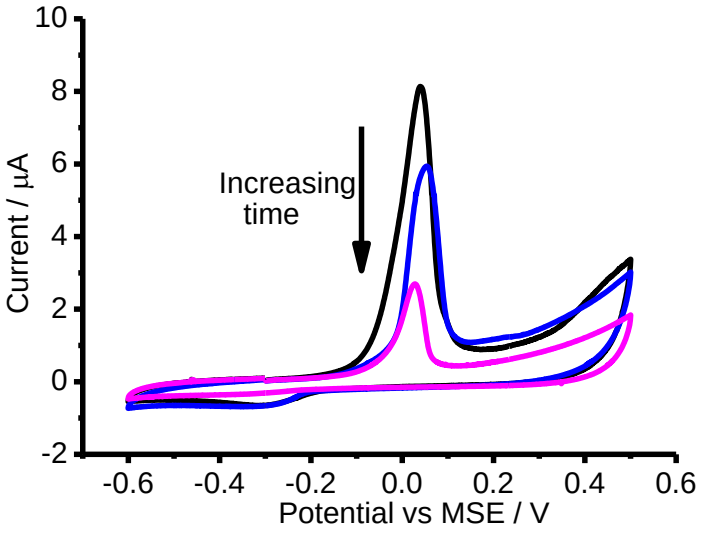


Figure 8. The oxidative stripping of silver nanoparticles (radii = 4.7 ± 1.8 nm) from a glassy carbon electrode in 0.1 M sodium nitrate spiked with 5 µM cysteine with different exposure times recorded at a scan rate of 0.05 V $s^{-1}$. Black: CV recorded immediately; Blue: CV recorded after electrode was soaked for 60 minutes; Pink: CV recorded after electrode was soaked for 15 hours 15 minutes.

Next, time studies were performed by soaking a silver nanoparticle (radii = 4.7 ± 1.8 nm) modified electrode in degassed sodium nitrate containing 5 µM cysteine for a duration varying from 60 minutes to 945 minutes before a cyclic voltammetry was performed. The voltammograms are shown in Figure 8 and it was observed that there was an inverse

correlation between cysteine exposure time and the oxidative peak charge under the signal. Moreover, a constant oxidation potential but no split oxidation signals were observed for silver oxidation even after 16 hours of exposure to cysteine.

### 3.2.2 UV-vis spectroscopic data of silver nanoparticles in presence of cysteine

Both batches of the nanoparticles were diluted and UV-vis spectroscopy was performed when cysteine was added. Both cysteine concentration and exposure time were varied. The cysteine concentration study for the nanoparticles are summarised in Figure 9a and 9b. The time variation study was performed with nanoparticles of radii 4.7 ± 1.8 nm with 1mM cysteine and the spectrum is recorded in the Supporting Information Figure S8. Similar results were seen for both batches of silver nanoparticles for both concentration and time variation studies. There is a small drop in absorbance for the signal at 400 nm in the presence of cysteine. With increasing cysteine concentration, the absorbance signal remains effectively constant whilst with increasing exposure time, there is a small decrease in absorbance at 400nm. For all the UV-vis experiments, no new surface plasmon peak was observed.

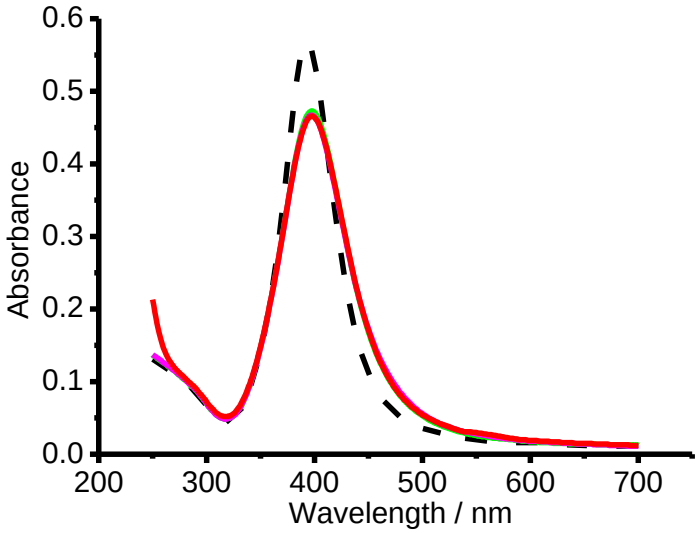


Figure 9a. UV-vis spectrum of silver nanoparticles (radii = 4.7 ± 1.8 nm) exposed to different concentrations of cysteine. Black dashed line: silver nanoparticles with no cysteine; Green: 5 µM; Pink: 10 µM; Red: 1 mM.

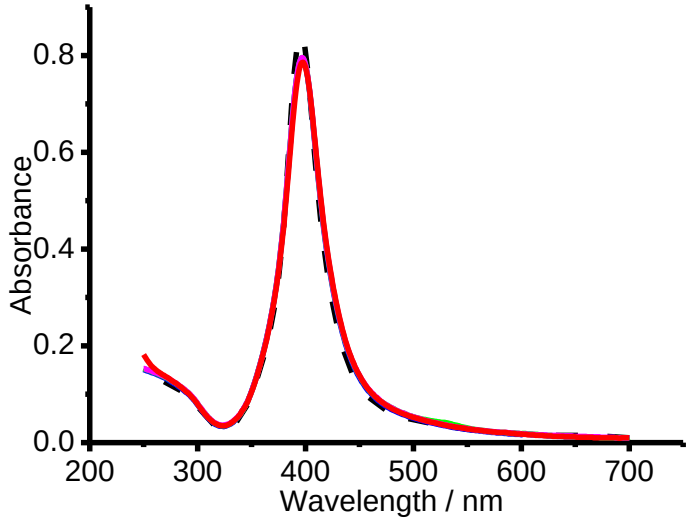


Figure 9b. UV-vis spectrum of silver nanoparticles (radii = 13.6 ± 3.7 nm) exposed to different concentrations of cysteine. Black dashed line: silver nanoparticle with no cysteine; Blue: 1 µM; Green: 5 µM; Pink: 10 µM; Red: 1 mM.

Consequently, there are three main observations for the behaviour of silver nanoparticles in the presence of cysteine which are to be accounted for:

I. The decreasing electrochemical oxidative charge and constant UV-vis absorbance signal with increasing cysteine concentration (Figure 7, 9a and 9b)

II. The constant electrochemical oxidation potential, the absence of split oxidation signals and the absence of a UV-vis absorbance signal at 500 – 600 nm with increasing cysteine concentration or increasing exposure time (Figure 6, 8, 9a and 9b)

III. The apparent absence of a size effect (Figure 7)

Applying the model hypothesized in the MH studies, the difference in behaviour between MH and cysteine is explained in the following sections.

### 3.2.3 The decreasing electrochemical oxidative charge and constant UV-vis absorbance signal with increasing cysteine concentration

With increasing cysteine concentration or increasing exposure time, the oxidative charge decreased. The amount of oxidative charge is linked to the amount of silver available for oxidation, hence, the amount of metallic silver available for oxidation on the electrode decreased. It was suggested in the MH studies (Section 3.1.2) that the decreasing oxidation charge with concentration and time was related to the formation of the silver(I) thiolate compound $AgSR_m$ from silver nanoparticles and MH. Following the mechanism of MH studies, if $AgSR_c$ (where $R_c$ = $-C_3H_6NO_2$) was formed continuously, the silver nanoparticles would get smaller. At this range of nanoparticle size, the extinction coefficient decreases with size, thus, the UV-vis spectrum should display a decrease in UV-vis absorbance with increasing cysteine concentration.[44,55] However, it is seen that the UV-vis absorbance signal at 400nm remained effectively constant in Figure 9a and 9b. Therefore, a mechanism which applies to cysteine is different from one which operates for MH. It is proposed that cysteine replaces the citrate capping agent around the silver nanoparticles to give cysteine-capped silver nanoparticles.[34] To prove the presence of cysteine capped nanoparticles, a control

experiment was performed by mixing silver nanoparticles (radii = 4.7 ± 1.8 nm) with cysteine and UV-vis spectra were recorded at different pH. The synthesized cysteine capped silver nanoparticles aggregated at pH 5.7 while maintaining their form at pH 6.9. This indicates that cysteine capped nanoparticles are formed when cysteine and silver nanoparticles are mixed.[34] No such behaviour occurred with citrate capped silver nanoparticles (see Supporting Information Figure S9 and S10).

In the UV-vis experiments, similar to the citrate capped silver nanoparticles, cysteine capped silver nanoparticles give an absorbance signal at 400 nm.[34] A slight drop in UV-vis absorbance corresponded to the oxidation of silver metal by cysteine to covalently attach itself to the silver nanoparticle. Assuming a thin layer formation of $AgSR_c$ on the silver nanoparticle surface to form the cysteine capping layer, a constant amount of silver is required to form the cysteine capped nanoparticles. Thus, the silver nanoparticle size drops slightly to a similar extent with a thin cysteine capping layer formed. Consequently, the absorbance signal recorded on the spectrum remains effectively constant as the cysteine concentration changes.

Speculating that a fixed amount of silver is consumed to form the cysteine capped nanoparticles, in the electrochemical experiments, the oxidative charge measured in the presence of cysteine should have remained effectively constant. However, it was observed in Figure 7 that the measured oxidative charge has an inverse relationship with cysteine concentration. A control experiment detailed in the Supporting Information Figure S11 shows that cysteine capped nanoparticles do not give an oxidation signal at the window of 0 V to +0.3 V vs MSE. Therefore, the cysteine capping agent might have either inactivated the silver surface, stopping silver oxidation or caused detachment of the nanoparticles from the

electrode. Both will cause the drop in electrochemical oxidative charge with increasing cysteine concentration. Hence, having cysteine capped silver nanoparticles as a product of silver nanoparticle-cysteine interaction can explain the constant absorbance signal and the decrease in the electrochemical oxidative charge measured.

### 3.2.4 The constant electrochemical oxidation potential, the absence of split oxidation signals and the absence of UV-vis absorbance signal at 500 – 600 nm with increasing cysteine concentration or increasing exposure time

It is surmised that cysteine forms a capping shell with inactivation of the nanoparticle surface or nanoparticle detachment from the electrode. Therefore, only the silver nanoparticles with incomplete replacement of citrate by cysteine contribute to the oxidative charges. Thus, despite the presence of cysteine, the kinetics of silver oxidation remained unaltered and the oxidation peak potential remained constant and no split oxidation signals was recorded. Therefore, in the UV-vis experiments, given that the solution consisted of citrate capped silver nanoparticles and cysteine capped silver nanoparticles, the species which caused an absorbance signal at 500 – 600 nm with MH is not present in the cysteine experiment. In short, the trends observed in the MH studies were not observed in the cysteine studies due to significant differences in the silver-thiol interactions.

### 3.2.5 The apparent absence of a size effect

As seen in Figure 9, two different sizes of nanoparticles of 4.7 ± 1.8 nm and 13.6 ± 3.7 nm were used in experiments. Due to the experimental inherent variability, it is not possible to show a significant size effect. From Section 3.1.7, the silver-thiol interaction is a diffusion

limited process where the high silver surface coverage ($4.2 \times 10^{-5}$ mol $m^{-2}$) causes a linear diffusion profile across the entire working electrode. Based on similar calculations in Section 3.1.7, it takes less than 10 milliseconds for sufficient cysteine to diffuse and cover the surface at 10 µM of cysteine. In the actual experiment, it takes even lesser time due to the convection caused by electrode insertion into the electrolyte. Therefore, within the short time scale that the linear diffusion profile is applicable, the amount of cysteine reaching the electrode surface is similar for both batches of nanoparticles. However, the kinetics of cysteine replacing citrate as capping agent are unknown. Moreover, the extent of how much cysteine replacement is needed to exhibit cysteine capped nanoparticles' characteristics is also unspecified. Thus, further detailed kinetics studies on how cysteine displaces citrate have to be attempted before the effects of the nanoparticle size can be explained and quantified in detail.

### 3.2.6 Summary on the interaction between silver nanoparticles and cysteine

In summary, cysteine interacts with silver nanoparticles in a way different from MH. Cysteine likely replaces the citrate capping agent and bonds covalently with silver nanoparticles to give a UV-vis absorbance signal at 400 nm. Therefore, in the UV-vis experiments, the silver nanoparticles had a size decrease to the same extent, causing an effectively constant absorbance at 400 nm with increasing cysteine concentrations. In the electrochemical experiments, the oxidative charge measured decreased with increasing cysteine concentrations. This was speculated to be an inactivation of silver surface through cysteine capping or the detachment of cysteine capped nanoparticles from the electrode surface.

## 4 Conclusions

The two thiols compounds studied, MH and cysteine, interacted with silver nanoparticles differently despite both having a sulfhydryl group as the primary structure motif. MH was suggested to form a sparingly soluble shell of $AgSR_m$ with silver, which remains on the nanoparticle surface, allowing further phase transition to occur. Both MH electrochemical and UV-spectroscopy data have shown an additional signal which is speculated to be due to formation of a compact layer of $AgSR_m$ and $Ag_2S$-like complexes via phase transition of initially formed $AgSR_m$ shell on the nanoparticle surface. In contrast, cysteine is surmised to displace the citrate capping agent to give cysteine capped nanoparticles, giving no split signals in both electrochemical and UV-vis spectroscopy. Instead, the change in capping agent can cause an inactivation of the nanoparticles or the detachment of the nanoparticles from the electrode surface. It is evident that no general mechanism for the interactions of thiol with silver nanoparticles exist and that each thiol should be treated individually.

## 5 Acknowledgements

HST is supported by the National Research Foundation Singapore under its National Research Foundation (NRF) Environmental and Water Technologies (EWT) PhD Scholarship Programme and administered by the Environment and Water Industry Programme Office (EWI). KT was supported by a Marie Curie Intra European Fellowship. CBM and RGC acknowledge funding from the European Union's Seventh Framework Programme (FP/2007-2013) / ERC Grant Agreement n. [320403].

## 6 References

(1) Riedel S ,Kaupp M. The highest oxidation states of the transition metal elements. Coordin Chem Rev, 2009, 253: 606-624.

(2) Lilienfeld S ,White CE. A Study of the Reaction between Hydrogen Sulfide and Silver. J Am Chem Soc, 1930, 52: 885-892.

(3) Graedel TE, Franey JP, Gualtieri GJ, Kammlott GW, Malm DL. On the mechanism of silver and copper sulfidation by atmospheric H2S and OCS. Corros Sci, 1985, 25: 1163-1180.

(4) Sinclair JD. Tarnishing of Silver by Organic Sulfur Vapors: Rates and Film Characteristics. J Electrochem Soc, 1982, 129: 33.

(5) Bell RA, Kramer JR. Structural chemistry and geochemistry of silver-sulfur compounds: Critical review. Environ Toxicol Chem, 1999, 18: 9-22.

(6) Dance IG, Fisher KJ, Banda RMH, Scudder ML. Layered Structure of Crystalline Compounds Agsr. Inorg Chem, 1991, 30: 183-187.

(7) Andersson L-O. Study of some silver-thiol complexes and polymers: Stoichiometry and optical effects. J Polym Sci A1, 1972, 10: 1963-1973.

(8) Musante C, White JC. Toxicity of silver and copper to Cucurbita pepo: differential effects of nano and bulk-size particles. Environ Toxicol, 2012, 27: 510-517.

(9) Batchelor-McAuley C, Tschulik K, Neumann CCM, Laborda E,Compton RG. Why are Silver Nanoparticles More Toxic Than Bulk Silver? Towards Understanding the Dissolution and Toxicity of Silver Nanoparticles. Int J Electrochem Sci, 2014, 9: 1132-1138.

(10) Leesutthiphonchai W, Dungchai W, Siangproh W, Ngamrojnavanich N, Chailapakul O. Selective determination of homocysteine levels in human plasma using a silver nanoparticle-based colorimetric assay. Talanta, 2011, 85: 870-876.

(11) Kunkalekar RK, Naik MM, Dubey SK, Salker AV. Antibacterial activity of silver-doped manganese dioxide nanoparticles on multidrug-resistant bacteria. J Chem Tech Biotechnol, 2013, 88: 873-877.

(12) Park Y, Noh HJ, Han L, Kim H-S, Kim Y-J, Choi JS, Kim C-K, Kim YS, Cho S. Artemisia capillaris Extracts as a Green Factory for the Synthesis of Silver Nanoparticles with Antibacterial Activities. J Nanosci Nanotechnol, 2012, 12: 7087-7095.

(13) Sureshkumar M, Siswanto DY, Lee C-K. Magnetic antimicrobial nanocomposite based on bacterial cellulose and silver nanoparticles. J Mater Chem, 2010, 20: 6948.

(14) Marambio-Jones C, Hoek EMV. A review of the antibacterial effects of silver nanomaterials and potential implications for human health and the environment. J Nanopart Res, 2010, 12: 1531-1551.

(15) Pradhan N, Pal A, Pal T. Silver nanoparticle catalyzed reduction of aromatic nitro compounds. Colloid Surface A, 2002, 196: 247-257.

(16) Esumi K, Isono R, Yoshimura T. Preparation of PAMAM− and PPI−Metal (Silver, Platinum, and Palladium) Nanocomposites and Their Catalytic Activities for Reduction of 4-Nitrophenol. Langmuir, 2004, 20: 237-243.

(17) Mitsudome T, Arita S, Mori H, Mizugaki T, Jitsukawa K, Kaneda K. Supported Silver-Nanoparticle-Catalyzed Highly Efficient Aqueous Oxidation of Phenylsilanes to Silanols. Angew Chem, 2008, 120: 8056-8058.

(18) Teo WZ, Pumera M. Fate of silver nanoparticles in natural waters; integrative use of conventional and electrochemical analytical techniques. RSC Advances, 2014, 4: 5006.

(19) Levard C, Hotze EM, Lowry GV, Brown GE, Jr. Environmental transformations of silver nanoparticles: impact on stability and toxicity. Environ Sci Technol, 2012, 46: 6900-6914.

(20) Lee PC, Meisel D. Adsorption and surface-enhanced Raman of dyes on silver and gold sols. J Phys Chem-US, 1982, 86: 3391-3395.

(21) Shang L, Dong S. Sensitive detection of cysteine based on fluorescent silver clusters. Biosens Bioelectron, 2009, 24: 1569-1573.

(22) Chen S, Gao H, Shen W, Lu C, Yuan Q. Colorimetric detection of cysteine using noncrosslinking aggregation of fluorosurfactant-capped silver nanoparticles. Sensor Actuat B, 2014, 190: 673-678.

(23) Tschulik K, Palgrave RG, Batchelor-McAuley C, Compton RG. 'Sticky electrodes' for the detection of silver nanoparticles. Nanotechnology, 2013, 24: 295502.

(24) Zhu J, Song X, Gao L, Li Z, Liu Z, Ding S, Zou S, He Y. A highly selective sensor of cysteine with tunable sensitivity and detection window based on dual-emission Ag nanoclusters. Biosens Bioelectron, 2014, 53: 71-75.

(25) Samberg ME, Oldenburg SJ, Monteiro-Riviere NA. Evaluation of silver nanoparticle toxicity in skin in vivo and keratinocytes in vitro. Environ Health Perspect, 2010, 118: 407-413.

(26) AshaRani PV, Low GKM, Hande MP, Valiyaveettil S. Cytotoxicity and genotoxicity of silver nanoparticles in human cells. ACS Nano, 2009, 3: 279-290.

(27) Kim YS, Kim JS, Cho HS, Rha DS, Kim JM, Park JD, Choi BS, Lim R, Chang HK, Chung YH, Kwon IH, Jeong J, Han BS, Yu IJ. Twenty-eight-day oral toxicity, genotoxicity, and gender-related tissue distribution of silver nanoparticles in Sprague-Dawley rats. Inhal Toxicol, 2008, 20: 575-583.

(28) Ansar SM, Perera GS, Gomez P, Salomon G, Vasquez ES, Chu IW, Zou S, Pittman CU, Walters KB, Zhang D. Mechanistic Study of Continuous Reactive Aromatic Organothiol Adsorption onto Silver Nanoparticles. J Phys Chem C, 2013, 117: 27146-27154.

(29) Andrieux-Ledier A, Tremblay B, Courty A. Stability of self-ordered thiol-coated silver nanoparticles: oxidative environment effects. Langmuir, 2013, 29: 13140-13145.

(30) Battocchio C, Meneghini C, Fratoddi I, Venditti I, Russo MV, Aquilanti G, Maurizio C, Bondino F, Matassa R, Rossi M, Mobilio S, Polzonetti G. Silver Nanoparticles Stabilized with Thiols: A Close Look at the Local Chemistry and Chemical Structure. J Phys Chem C, 2012, 116: 19571-19578.

(31) Levard C, Hotze EM, Colman BP, Dale AL, Truong L, Yang XY, Bone AJ, Brown GE, Jr., Tanguay RL, Di Giulio RT, Bernhardt ES, Meyer JN, Wiesner MR, Lowry GV. Sulfidation of silver nanoparticles: natural antidote to their toxicity. Environ Sci Technol, 2013, 47: 13440-13448.

(32) Kim B, Park CS, Murayama M, Hochella MF. Discovery and characterization of silver sulfide nanoparticles in final sewage sludge products. Environ Sci Technol, 2010, 44: 7509-7514.

(33) Zhang N, Qu F, Luo HQ, Li NB. Sensitive and selective detection of biothiols based on target-induced agglomeration of silver nanoclusters. Biosens Bioelectron, 2013, 42: 214-218.

(34) Csapo E, Patakfalvi R, Hornok V, Toth LT, Sipos A, Szalai A, Csete M, Dekany I. Effect of pH on stability and plasmonic properties of cysteine-functionalized silver nanoparticle dispersion Colloid Surface B, 2012, 98: 43-49.

(35) Li H, Cui Z, Han C. Glutathione-stabilized silver nanoparticles as colorimetric sensor for Ni2+ ion. Sensor Actuat B: Chem, 2009, 143: 87-92.

(36) Lyons J, Rauh-Pfeiffer A, Yu YM, Lu XM, Zurakowski D, Tompkins RG, Ajami AM, Young VR, Castillo L. Blood glutathione synthesis rates in healthy adults receiving a sulfur amino acid-free diet. Proc Natl Acad Sci U S A, 2000, 97: 5071-5076.

(37) Patterson RA, Lamb DJ, Leake DS. Mechanisms by which cysteine can inhibit or promote the oxidation of low density lipoprotein by copper. Atherosclerosis, 2003, 169: 87-94.

(38) Wan Y, Guo Z, Jiang X, Fang K, Lu X, Zhang Y, Gu N. Quasi-spherical silver nanoparticles: aqueous synthesis and size control by the seed-mediated Lee-Meisel method. J Colloid Interface Sci, 2013, 394: 263-268.

(39) Toh HS, Batchelor-McAuley C, Tschulik K, Damm C, Compton RG. A proof-of-concept – Using pre-created nucleation centres to improve the limit of detection in anodic stripping voltammetry. Sensor Actuat B: Chem, 2014, 193: 315-319.

(40) Lees JC, Ellison J, Batchelor-McAuley C, Tschulik K, Damm C, Omanovic D, Compton RG. Nanoparticle impacts show high-ionic-strength citrate avoids aggregation of silver nanoparticles. Chemphyschem, 2013, 14: 3895-3897.

(41) Haynes WM, Lide DR, Bruno TJ CRC Handbook of Chemistry and Physics 2012-2013; 93rd ed.; Taylor & Francis Group: Florida, 2012.

(42) Toh HS, Batchelor-McAuley C, Tschulik K, Compton RG. Electrochemical detection of chloride levels in sweat using silver nanoparticles: a basis for the preliminary screening for cystic fibrosis. Analyst, 2013, 138: 4292-4297.

(43) Henglein A, Mulvaney P, Linnert T. Chemistry of Ag n aggregates in aqueous solution: non-metallic oligomeric clusters and metallic particles. Faraday Discussions, 1991, 92: 31.

(44) Evanoff DD,Chumanov G. Size-Controlled Synthesis of Nanoparticles. 2. Measurement of Extinction, Scattering, and Absorption Cross Sections. J Phys Chem B, 2004, 108: 13957-13962.

(45) Mock JJ, Barbic M, Smith DR, Schultz DA, Schultz S. Shape effects in plasmon resonance of individual colloidal silver nanoparticles. J Chem Phys, 2002, 116: 6755-6759.

(46) Mulvaney P, Giersig M, Henglein A. Electrochemistry of multilayer colloids: preparation and absorption spectrum of gold-coated silver particles. J Phys Chem, 1993, 97: 7061-7064.

(47) Kelly KL, Coronado E, Zhao LL, Schatz GC. The Optical Properties of Metal Nanoparticles: The Influence of Size, Shape, and Dielectric Environment. J Phys Chem B, 2003, 107: 668-677.

(48) Kuzma A, Weis M, Flickyngerova S, Jakabovic J, Satka A, Dobrocka E, Chlpik J, Cirak J, Donoval M, Telek P, Uherek F, Donoval D. Influence of surface oxidation on plasmon resonance in monolayer of gold and silver nanoparticles. J Appl Phys, 2012, 112: 103531.

(49) Krzewska S, Podsiadły H. Complexes of Ag(I) with ligands containing sulphur donor atoms. Polyhedron, 1986, 5: 937-944.

(50) Levard C, Reinsch BC, Michel FM, Oumahi C, Lowry GV, Brown GE. Sulfidation processes of PVP-coated silver nanoparticles in aqueous solution: impact on dissolution rate. Environ Sci Technol, 2011, 45: 5260-5266.

(51) Toh HS, Batchelor-McAuley C, Tschulik K, Uhlemann M, Crossley A, Compton RG. The anodic stripping voltammetry of nanoparticles: electrochemical evidence for the surface agglomeration of silver nanoparticles. Nanoscale, 2013, 5: 4884-4893.

(52) Davies TJ, Compton RG. The cyclic and linear sweep voltammetry of regular and random arrays of microdisc electrodes: Theory. J Electroanal Chem, 2005, 585: 63-82.

(53) Kätelhön E, Cheng W, Batchelor-McAuley C, Tschulik K, Compton RG. Nano-impact experiments are highly sensitive to the presence of adsorbed species on electrode surfaces. ChemElectroChem, 2014, DOI: 10.1002/celc.201402014.

(54) Ward Jones SE, Campbell FW, Baron R, Xiao L, Compton RG. Particle Size and Surface Coverage Effects in the Stripping Voltammetry of Silver Nanoparticles: Theory and Experiment. J Phys Chem C, 2008, 112: 17820-17827.

(55) Evanoff DD, Jr., Chumanov G. Synthesis and optical properties of silver nanoparticles and arrays. Chemphyschem, 2005, 6: 1221-1231.

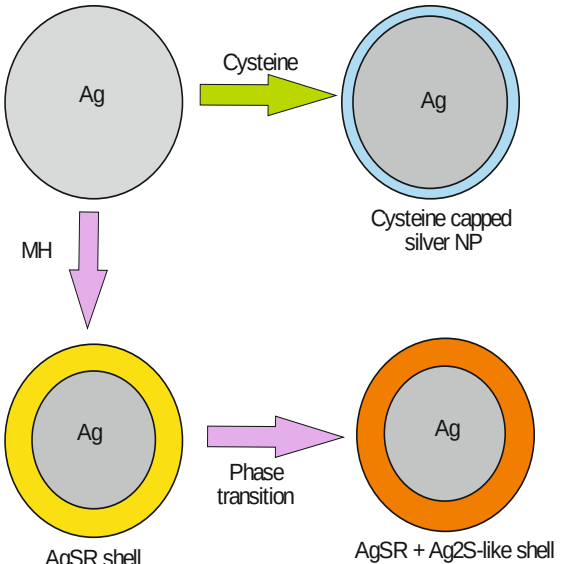

Table of Content Graphic